2008 IEEE International Conference on
Robotics and Automation
Pasadena, CA, USA, May 19-23, 2008

Concurrent Multi-Link Deployment of a Gravity-Assisted Underactuated Snake Robot for Aircraft Assembly

Binayak Roy and H. Harry Asada
d'Arbeloff Laboratory for Information Systems and Technology
Department of Mechanical Engineering
Massachusetts Institute of Technology
Cambridge, MA 02139, USA
{binayak,asada}@mit.edu

***Abstract*— This paper presents algorithms for concurrent deployment of multiple links of a gravity-assisted underactuated robot arm. The joints of the hyper-articulated arm have no dedicated actuators, but are activated with gravity. By tilting the base link appropriately, multiple unactuated links may be steered simultaneously to desired angular positions. This underactuated arm design was motivated by the need for a compact snake-like robot that can go into aircraft wings and perform assembly operations using heavy end-effecters. The dynamics of the unactuated links are essentially 2^{nd} order non-holonomic constraints, for which there are no general control algorithms. We perform a controllability analysis to establish the feasibility of multi-link positioning using the available inputs, viz., the biaxial tilts of the base link. We propose a feed-forward control algorithm for simultaneous positioning of multiple links. We also propose an intermittent feedback control scheme to compensate for disturbances acting on the system. We built a 4 link prototype where the base is tilted using a Stewart Platform. The proposed control schemes are implemented on our prototype system. The experimental results indicate the efficacy of the control schemes.**

I. Introduction

Most assembly operations in aircraft manufacturing are currently done manually. Although aircraft are small in lot size, numerous repetitive assembly operations have to be performed on a single aircraft. The conditions are often ergonomically challenging and these result in low productivity as well as frequent injuries. Thus, there is a need to shift from manual assembly to automated robotic assembly. The following wing-box assembly illustrates this.

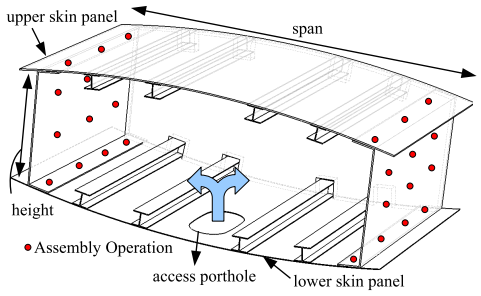

Fig. 1. Cross section of an aircraft wing

Fig. 1 shows a cross-section of an aircraft wing. Several assembly operations, such as burr-less drilling and fastener installations, have to be carried out inside the wing after the *upper* and *lower skin panels* are in place. The interior of the wing is accessible **only** through small portholes along its length. These *access portholes* are roughly elliptical with dimensions of 0.46 m (18 in) by 0.25 m (10 in). The wing also has a substantial *span*, which varies from 0.9 m (36 in) to 3 m (120 in) depending upon the size of the aircraft. The *height* of the section varies from about 0.2 m (8 in) to 0.9 m (36 in), depending upon the size of the aircraft, as well as the location of the wing-section along the length of the wing. Presently, the assembly operations are carried out manually. A worker enters the wing-box through the small portholes and lies flat on the base, while carrying out the assembly operations. Evidently, the working conditions are ergonomically challenging.

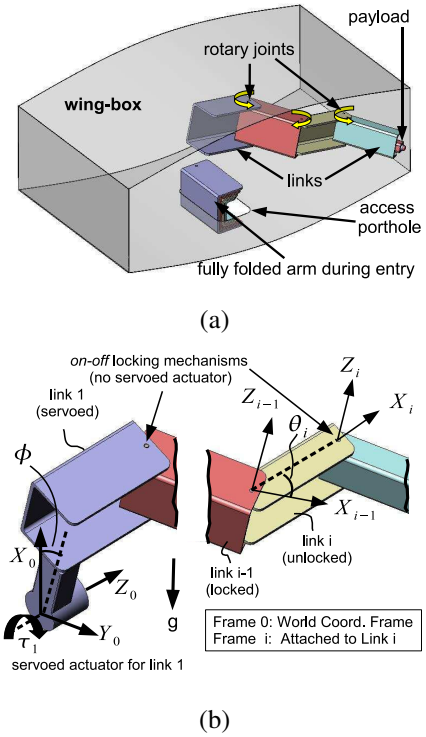

Fig. 2. Previous Work: (a) Structure of robot arm; (b) Actuation scheme

We have proposed a "nested-channel" serial linkage mechanism capable of operating inside an aircraft wing-box

[1]. The links are essentially C-channels with successively smaller base and leg lengths, as shown in Fig. 2(a). The adjacent links are connected by revolute joints, the axes of which are parallel. The use of channel structures is advantageous for a number of reasons. The channels can fold into each other resulting in an extremely compact structure during entry through the porthole. Once inside the wing-box, the links may be deployed to access distal points in the assembly space. The open channel structure also facilitates the attachment of a payload to the last link without increasing the overall dimensions of the arm.

The lack of a compact, powerful and high stroke actuation mechanism is the primary bottleneck in the development of the hyper articulated arm. In our previous work [1], we have proposed an underactuated design concept, which obviates the use of dedicated actuators for each joint. Instead, we utilize gravity for driving individual joints. This drastically reduces the size and weight of the manipulator arm.

The reconfiguration scheme is illustrated in Fig. 2(b), which shows a schematic of an n-link robot arm. The base link (link 1) is the only servoed link. It may be rotated about a **fixed axis** Z_0, which is orthogonal to the direction of gravity. All other joint axes (Z_j, $j \neq 0$) are orthogonal to Z_0. They are equipped with simple *on-off* locking mechanisms only. The goal is to rotate link i about Z_{i-1} by actuating link 1 appropriately. All unactuated links except link i are locked. Link 1 starts in the vertical upright position. Then it is rotated, first clockwise and then counter-clockwise, before being brought back to its vertical position. This tends to accelerate and then decelerate link i due to gravity and dynamic coupling with link 1. By controlling the tilting angle of link 1, link i can be brought to a desired position with zero velocity. Link i may be locked thereafter. This procedure can be repeated sequentially for the other unactuated links. Contraction of the arm can be performed by reversing the above deployment procedure.

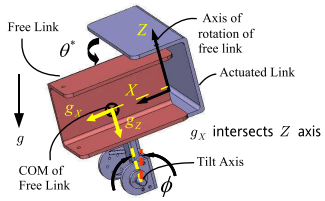

Fig. 3. Singular configuration

Based on the above "fixed axis of tilt" design, we have proposed control schemes suitable for sequential single-link deployment [1], [2]. However, there are two key limitations to the "fixed axis of tilt" design. Firstly, the speed of response of the unactuated links diminishes in configurations where the gravitational torque is near zero. This is shown in Fig. 3. Secondly, this design is geared towards sequential single-link deployment, where only a single joint is unlocked at any given time. Multiple links, however, can be deployed concurrently if the base is tilted about two orthogonal axes. Equivalently, the axis of tilt of the base is chosen *arbitrarily* in the horizontal plane. This modified design can reduce the deployment time and improve productivity and maneuverability of the hyper-articulated arm.

Previous research in underactuated manipulators deals mostly with the planar (vertical or horizontal) case where the actuated and unactuated joint axes are parallel [3]–[5]. In our approach, the actuated and unactuated joints are orthogonal and we can modulate the effect of gravity by controlling the actuated joint. Also, the arm operates in a confined space and only small motions of the base joint are permitted. Moreover, our control objective is simultaneous positioning of multiple free links. The special kinematic structure of our mechanism, the operational constraint and the control objective preclude the use of existing techniques developed in [3], [6]–[8].

This paper presents a new design concept for concurrent multi-link deployment of an underactuated hyper-articulated arm using a biaxial tilting table. Furthermore, we analyze the system dynamics to develop a simple model that captures the dominant dynamical effects. We then establish the controllability of the system based on the proposed dynamical model and the available inputs. Next, we propose a feed-forward control scheme for concurrent multi-link positioning. Thereafter, we propose an intermittent feedback control scheme where the feed-forward control law is updated based on periodic measurements of the outputs of the actual system. Finally, we present some simulation and experimental results to demonstrate the efficacy of our control algorithms.

II. Design Concept

Fig. 4 shows a schematic of our design concept. The Stewart Platform mechanism operates outside the wing-box and is used to deploy the links of the hyper-articulated arm. Z_0^* denotes a fixed reference direction in the horizontal plane. By coordinating the motion of the six legs of the hexapod, the table may be tilted about an arbitrary axis Z_0 in the horizontal plane. Link 1 is coupled directly to the hexapod table. Links 2, 3 and 4 are unactuated and the link joints are equipped with *on-off* electromagnetic brakes.

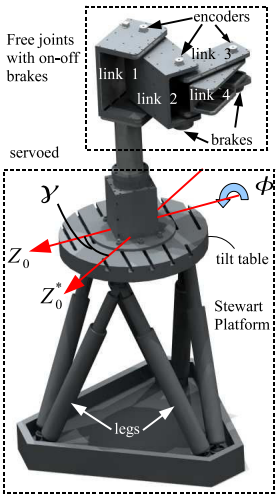

Fig. 4. Arbitrary axis of tilt using hexapod

It may be noted that any mechanism with biaxial tilt capability may be used for deployment. The Stewart Platform offers additional benefits, such as translational motion of the table, and is useful for maneuvering the arm inside the wing.

III. Dynamic Modeling

We consider the case where two unactuated links of the hyper-articulated arm are in motion concurrently. Fig. 5 shows a schematic of this setup. Link 1 (not shown) is the actuated link, and links 2 and 3 are unactuated. The axis of tilt is located on the horizontal plane and is denoted by Z_0. It is oriented at an angle γ with respect to the link 1 frame X_1Y_1. The tilt angle is denoted by ϕ. The points C_2 and C_3 denote the locations of the center of mass of links 2 and 3 respectively. The masses of links 2 and 3 are denoted by m_2 and m_3 respectively. I_{zz2} and I_{zz3} denote the centroidal inertias of links 2 and 3 respectively.

As with the case of sequential link deployment [2], we make the following assumptions:

1) Centrifugal and Coriolis coupling with link 1 (actuated link) is negligible.
2) Inertial coupling with link 1 is negligible.

It may be noted that the inertial coupling between links 2 and 3, as well as the centrifugal and Coriolis effects within the plane of links 2 and 3 are retained. We essentially end up with a double pendulum whose dynamics is modulated by gravity through a choice of the axis of tilt Z_0 (in the horizontal plane) and the tilt angle ϕ.

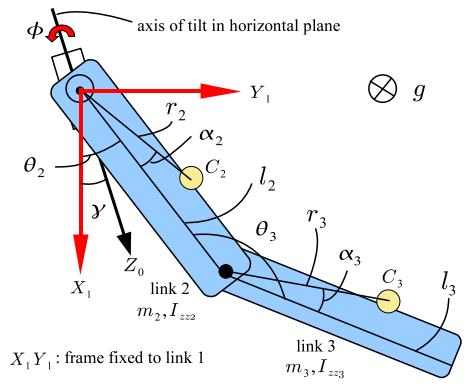

Fig. 5. Double pendulum in modulated gravity field

Let $q = [\theta_2, \theta_3]^T$ denotes the 2 dimensional vector of unactuated coordinates. The system dynamics for this approximate model may be written as:

$$H(q)\ddot{q} + C(q,\dot{q}) + G(\phi,\gamma,q) = 0. \tag{1}$$

Here

$$H = \begin{bmatrix} H_{22} & H_{23} \\ H_{23} & H_{33} \end{bmatrix},$$
$$H_{22}(q) = m_2 r_2^2 + m_3(l_2^2 + r_3^2 - 2l_2 r_3 \cos(\theta_3 - \alpha_3)) + I_{zz2} + I_{zz3},$$
$$H_{23}(q) = m_3 r_3 (l_2 \cos(\theta_3 - \alpha_3) - r_3),$$
$$H_{33}(q) = m_3 r_3^2 + I_{zz3},$$
$$G = \begin{bmatrix} G_2(\phi,\gamma,q) & G_3(\phi,\gamma,q) \end{bmatrix}^T,$$
$$G_2 = (m_2 r_2 \cos(\theta_2 + \alpha_2 - \gamma) + m_3 l_2 \cos(\theta_2 - \gamma) - m_3 r_3 \cos(\theta_2 - \theta_3 + \alpha_3 - \gamma))g \sin\phi,$$
$$G_3 = m_3 r_3 \cos(\theta_2 - \theta_3 + \alpha_3 - \gamma) g \sin\phi,$$
$$C(q,\dot{q}) = \dot{H}\dot{q} - \frac{1}{2}\frac{\partial}{\partial q}\dot{q}^T H \dot{q}.$$

The quantities l_2, r_2, r_3 are shown in Fig. 5. This simplified dynamical model is used as the basis of our concurrent multi-link deployment algorithms presented in Section V.

Remark 1: Although inertial and centrifugal coupling with link 1 have been neglected, the dynamical system (1) is still second-order non-holonomic. The gravity term is a function of the generalized coordinates θ_2, θ_3 and ϕ. Therefore it satisfies the conditions for 2^{nd} order non-holonomic systems stated in [9].

IV. Controllability Analysis

A. Linearized Analysis

We check the sufficient condition for local controllability by linearizing the system dynamics (1) about an equilibrium point in the state space. Let us define the state as $x = [\dot{\theta}_2, \dot{\theta}_3, \theta_2, \theta_3]^T$. It is convenient to redefine the inputs ϕ and γ as

$$u \triangleq [\phi_X, \phi_Y]^T \triangleq [\phi\cos\gamma, \phi\sin\gamma]^T \tag{2}$$

We linearize the system dynamics (1) about $(\dot{\theta}_2, \dot{\theta}_3, \theta_2, \theta_3, \phi_X, \phi_Y) = (0, 0, \bar{\theta}_2, \bar{\theta}_3, 0, 0)$, where $\bar{\theta}_2$, and $\bar{\theta}_3$ are arbitrary. The linearization is given by:

$$\delta\dot{x} = A\delta x - B\delta u. \tag{3}$$

Here

$$A = \begin{bmatrix} 0_{2\times 4} \\ I_{2\times 2} \quad 0_{2\times 2} \end{bmatrix},$$
$$B = \begin{bmatrix} N_{22}g_{23x} + N_{23}g_{3x} & N_{22}g_{23y} + N_{23}g_{3y} \\ N_{23}g_{23x} + N_{33}g_{3x} & N_{23}g_{23y} + N_{33}g_{3y} \\ 0_{2\times 2} \end{bmatrix},$$
$$[N] = [H]^{-1},$$
$$g_{23x} = m_2 g r_2 \cos(\theta_2 + \alpha_2) - m_3 g(r_3 \cos(\theta_2 - \theta_3 + \alpha_3) - l_2 \cos\theta_2),$$
$$g_{23y} = m_2 g r_2 \sin(\theta_2 + \alpha_2) - m_3 g(r_3 \sin(\theta_2 - \theta_3 + \alpha_3) - l_2 \sin\theta_2),$$
$$g_{3x} = m_3 g r_3 \cos(\theta_2 - \theta_3 + \alpha_3),$$
$$g_{3y} = m_3 g r_3 \sin(\theta_2 - \theta_3 + \alpha_3).$$

The controllability matrix is given by:

$$P = \begin{bmatrix} B & AB & A^2B & A^3B \end{bmatrix} = \left[\begin{array}{cccc|c} B_{11} & B_{12} & 0 & 0 & \\ B_{21} & B_{22} & 0 & 0 & \\ 0 & 0 & B_{11} & B_{12} & 0_{4\times 4} \\ 0 & 0 & B_{21} & B_{22} & \end{array}\right]. \quad (4)$$

Using the **Kalman rank condition**, the linearized system is controllable except when

$$B_{11}B_{22} - B_{12}B_{21} = 0 \Rightarrow \frac{g_{23y}}{g_{23x}} = \frac{g_{3y}}{g_{3x}}. \quad (5)$$

Thus, the dynamical system (1) satisfies the sufficient condition for local controllability, except in certain special configurations in the state space. A non-linear analysis using Sussmann's sufficient conditions [10] may be conclusive in such configurations. This will be addressed in future work.

B. Physical Interpretation

In this section, we present an intuitive understanding of the controllability analysis from the previous section. See Fig. 6. The point C_{23} denotes the combined center-of-mass of links 2 and 3. The point C_3 denotes the location of the center-of-mass of link 3. The goal is to achieve *in-phase* and *out-of-phase* steering for the free links. We define *in-phase* steering as the case where links 2 and 3 move in the same direction, viz. clockwise or counter-clockwise. Similarly, we define *out-of-phase* steering as the case where links 2 and 3 move in opposite directions.

Fig. 6(a) shows the choice of the orientation γ of the tilt axis O_2Z_0, such that *in-phase* steering may be achieved. The effective direction of gravity in the instantaneous plane of motion is given by OG. It may be noted that OG is orthogonal to O_2Z_0. The direction O_2G_2 (respectively, O_3G_3) is parallel to OG and denotes the direction of gravity as viewed from joint 2 (respectively, 3). It is evident from the figure that the gravitational torques on the free joints enable *in-phase* steering. Similarly, Fig. 6(b) shows the choice of the orientation γ of the tilt axis O_2Z_0, such that *out-of-phase* steering may be achieved.

The condition (5) corresponds to the case where O_2C_{23} and O_3C_3 are *parallel* or *anti-parallel*. When O_2C_{23} and O_3C_3 are *parallel*, the effective direction of gravity is the same relative to links 2 and 3. Thus, *out-of-phase* steering cannot be achieved. Similarly, *in-phase* steering cannot be achieved when O_2C_{23} and O_3C_3 are *anti-parallel*. Indeed, the quantities g_{23x} and g_{23y} in (5) may be identified with the x and y coordinates of the combined center-of-mass of links 2 and 3, i.e., the point C_{23}. Similarly, the quantities g_{3x} and g_{3y} may be identified with the x and y coordinates of the center-of-mass of link 3, i.e., the point C_3.

V. Feed-forward Control

Our goal is to concurrently steer 2 links from their respective initial locations (starting at 0 velocity) to desired final locations with zero final velocity. The corresponding boundary conditions may be written as ($i = 2, 3$)

$$\theta_i(0) = \theta_{i0},\ \theta_i(t_f) = \theta_{if} \text{ and } \dot{\theta}_i(0) = 0,\ \dot{\theta}_i(t_f) = 0. \quad (6)$$

Equations (1) and (6) represent a system of 4^{th} order ODEs with 8 boundary conditions. This problem may be formulated as a boundary value problem if the control input ϕ is parameterized in terms of 4 parameters. These parameters p_j ($1 \le j \le 4$) are constant but unknown and the system (1) and (6) may be augmented with the system

$$\dot{p}_j = 0. \quad (7)$$

We propose an algorithm for formalizing this approach.

We parameterize the tilt of link 1 along two fixed orthogonal axes, X_0^* and Y_0^* in the horizontal plane. Let us denote the angular rotations by ϕ_X and ϕ_Y respectively. See Fig. 7. The trajectories ϕ_X and ϕ_Y comprise three sigmoidal segments each. The parameters correspond to the peaks and troughs of the sigmoidal segments and are denote by ϕ_{Xa}, ϕ_{Xb}, ϕ_{Ya} and ϕ_{Yb}. For finite angular rotations, the sequence of rotations determines the final orientation of a rigid body.

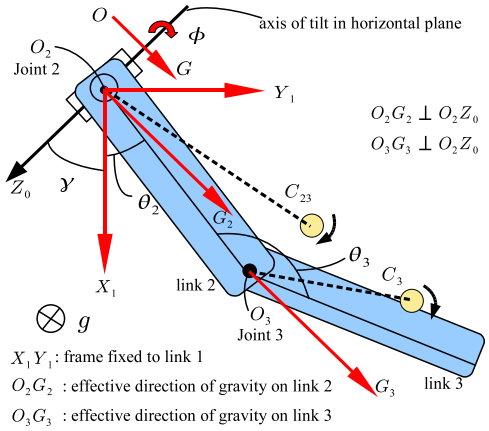

(a)

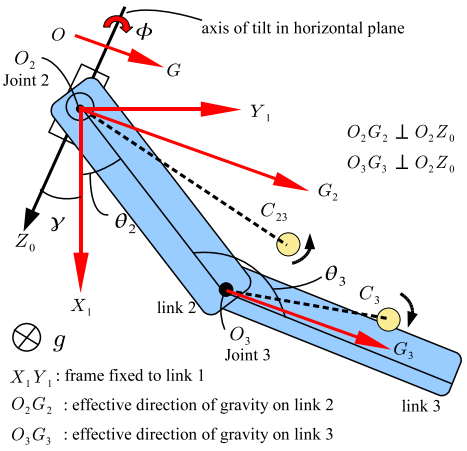

(b)

Fig. 6. Multi-link Steering: (a) In Phase Steering; (b) Out of Phase Steering

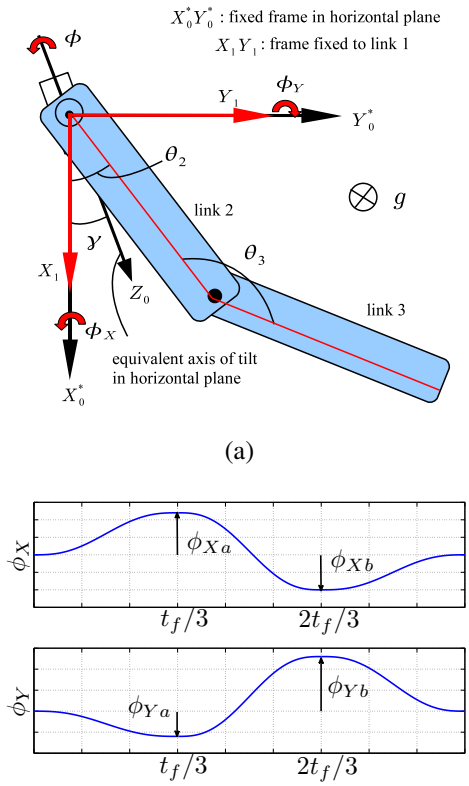

Fig. 7. Tilt Scheme for Concurrent Multi-link Deployment

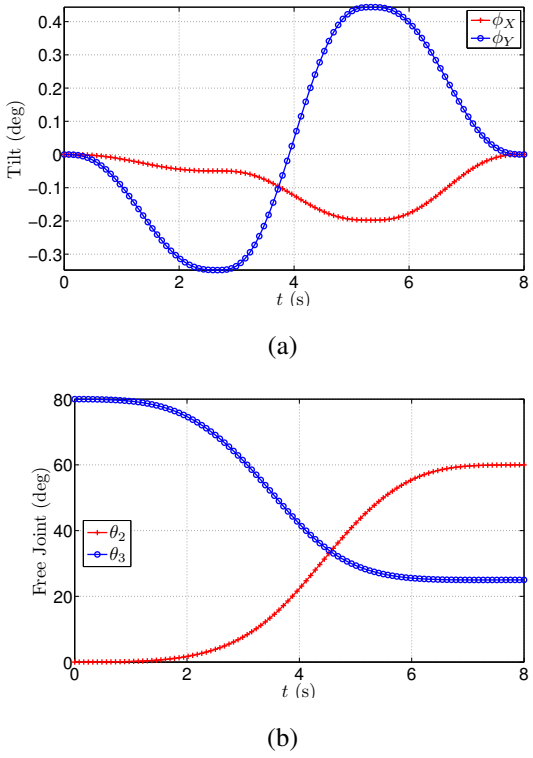

Fig. 8. In-phase motion: (a) Tilting table trajectories (ϕ_X and ϕ_Y); (b) Free joint trajectories

However, if $|\phi_X|$ and $|\phi_Y|$ are small, the rotations commute up to first order. We verify *a posteriori*, that this small angle assumption is indeed true. See *Remark 2*.

The orientation γ of the equivalent axis of tilt and the amplitude of tilt ϕ are give by

$$\gamma = \text{atan2}(\phi_Y, \phi_X) \text{ and } \phi = \sqrt{\phi_X^2 + \phi_Y^2}.$$

The duration of each sigmoidal segment was fixed at $\frac{t_f}{3}$. As a result, the orientation γ of the axis of tilt remains fixed during each subinterval $(0, \frac{t_f}{3})$, $(\frac{t_f}{3}, \frac{2t_f}{3})$ and $(\frac{2t_f}{3}, t_f)$. These fixed orientations are given by $\gamma_a = \text{atan2}(\phi_{Ya}, \phi_{Xa})$, $\gamma_b = \text{atan2}(\phi_{Yb} - \phi_{Ya}, \phi_{Xb} - \phi_{Xa})$ and $\gamma_a = \text{atan2}(-\phi_{Yb}, -\phi_{Xb})$.

Example 1: Fig. 8 shows the simulation results for the boundary conditions

$$\theta_2(0) = 0^\circ,\ \theta_2(t_f) = 60^\circ \text{ and } \theta_3(0) = 80^\circ,\ \theta_3(t_f) = 25^\circ.$$
$$\dot{\theta}_2(0) = 0,\ \dot{\theta}_2(t_f) = 0 \text{ and } \dot{\theta}_3(0) = 0,\ \dot{\theta}_3(t_f) = 0.$$

These boundary conditions correspond to *in-phase* motion of links 2 and 3 (both clockwise). The final time was set at $t_f = 8s$. Fig. 8(a) shows the X and Y components of the trajectories of the link 1. The parameters of the sigmoid trajectories obtained from the solution of the boundary value problem are

$$\phi_{Xa} = -0.05^\circ, \phi_{Xb} = -0.20^\circ, \phi_{Ya} = -0.35^\circ, \phi_{Yb} = 0.44^\circ.$$

Example 2: Fig. 9 shows the simulation results for the boundary conditions

$$\theta_2(0) = 0^\circ,\ \theta_2(t_f) = 80^\circ \text{ and } \theta_3(0) = 0^\circ,\ \theta_3(t_f) = 90^\circ.$$
$$\dot{\theta}_2(0) = 0,\ \dot{\theta}_2(t_f) = 0 \text{ and } \dot{\theta}_3(0) = 0,\ \dot{\theta}_3(t_f) = 0.$$

These boundary conditions correspond to *out-of-phase* motion of links 2 and 3 (link 2 counter-clockwise, link 3 clockwise). The final time was set at $t_f = 8s$. Fig. 9(a) shows the X and Y components of the trajectories of the link 1. The parameters of the sigmoid trajectories obtained from the solution of the boundary value problem are

$$\phi_{Xa} = -0.39^\circ, \phi_{Xb} = 0.38^\circ, \phi_{Ya} = -0.38^\circ, \phi_{Yb} = 0.32^\circ.$$

Remark 2: In both cases the amplitudes of tilt are small. This verifies, *a posteriori*, the small angle assumption ensuring commutativity of rotations.

VI. Experimental Results

Fig. 10 shows a schematic of the prototype robot developed for aircraft manufacturing. The links are deployed using a Stewart Platform (hexapod), which is shown in Fig. 10(a). The legs of the hexapod are actuated by means of AC servomotors coupled to linear ball screw mechanisms. The hexapod table is equipped with a dual-axis MEMS tilt sensor for determining its absolute orientation with respect to the direction of gravity. The hexapod table interfaces with Link 1 of the hyper-articulated mechanism through a coupling, as shown in Fig. 10(b). The link mechanism, which operates

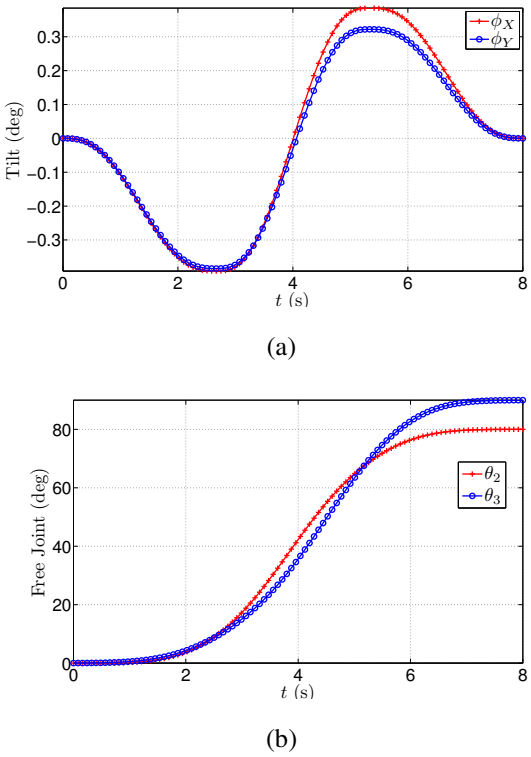

Fig. 9. Out-of-Phase motion: (a) Tilting table trajectories (ϕ_X and ϕ_Y); (b) Free joint trajectories

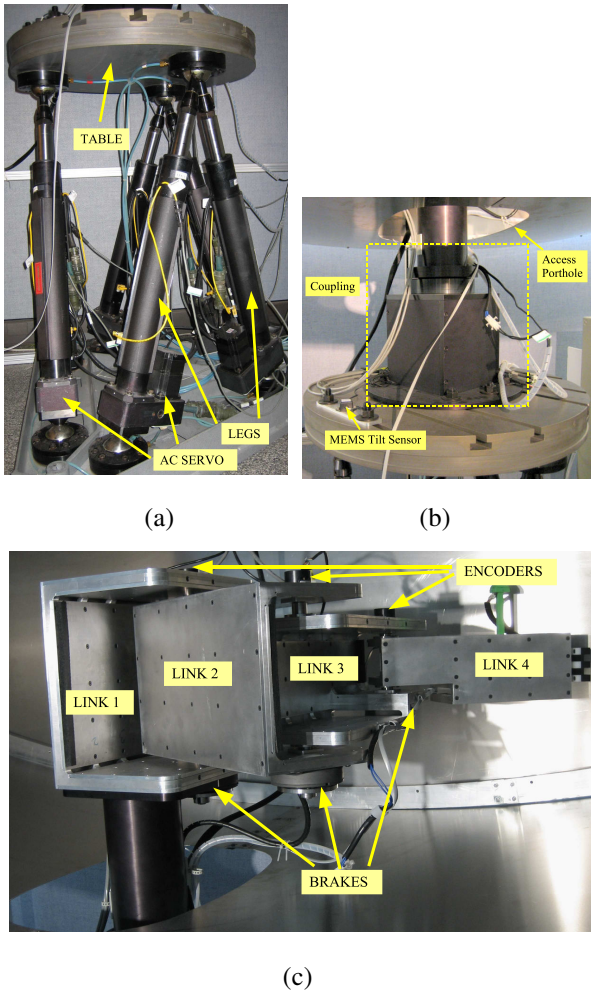

Fig. 10. Prototype 4 link system: (a) Stewart Platform; (b) Table-link coupling; (c) Link mechanism

inside the wing-box, is shown in Fig. 10(c). Links 2, 3 and 4 are equipped with *on-off* electromagnetic brakes rated at 50 N-m, 25 N-m and 12 N-m respectively. The relative angular position of the links are measured using optical encoders with a resolution of 1000 pulses per revolution.

We conducted position control experiments on the prototype system to verify the control algorithms for concurrent multi-link deployment. We verify the theoretical predictions for both *in-phase* and *out-of-phase* motion. Fig. 11(a) shows the experimental results for *in-phase* motion. The boundary conditions and duration of motion are identical to those of the simulation results presented in Fig. 8. Fig. 11(b) shows the experimental results for *out-of-phase* motion. The boundary conditions and duration of motion correspond to the simulation results presented in Fig. 9. The actual final positions were $[\theta_2(t_f), \theta_3(t_f)] = [56.25°, 29.97°]$ for *in-phase* motion and $[\theta_2(t_f), \theta_3(t_f)] = [77.58°, 90.45°]$ for *out-of-phase* motion. The experimental results show reasonable agreement with the theoretical predictions. The errors in the final positions may be attributed to unmodeled dynamical effects such as friction and presence of cables. These errors may be compensated by using the sequential closed-loop control scheme presented in [2].

VII. Conclusions and Future Work

In this paper, we presented algorithms for concurrent deployment of multiple links of a gravity-assisted underactuated robot arm. The joints of the hyper-articulated arm have no dedicated actuators, but are activated with gravity. By tilting the base link appropriately, multiple unactuated links may be steered simultaneously to desired angular positions. This underactuated arm design was motivated by the need for a compact snake-like robot that can go into aircraft wings and perform assembly operations using heavy end-effecters. We analyzed the system dynamics and created a simple model to facilitate control design. Next, we performed a controllability analysis to establish the feasibility of multi-link positioning using the available inputs, viz., the biaxial tilts of the base link. We proposed a feed-forward control algorithm for simultaneous positioning of multiple links. We built a 4 link prototype where the base is tilted using a Stewart Platform. Finally, we presented some experimental results using the feed-forward control algorithm.

Our analysis in this paper is limited to the case where two links are deployed simultaneously. Further, we only consider the case where the brakes are unlocked (at start) and locked (at finish) simultaneously. By switching the brakes on and off at different time instants, more than two links may be deployed concurrently. An interesting future direction

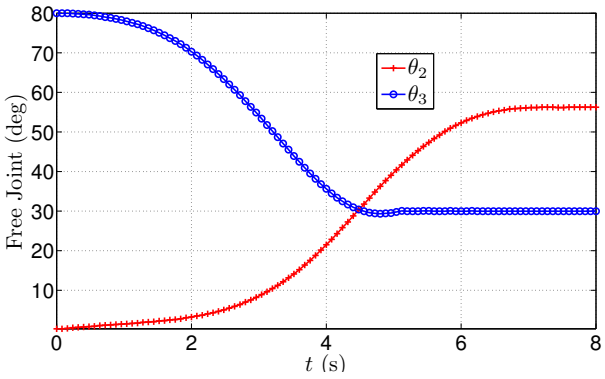

(a)

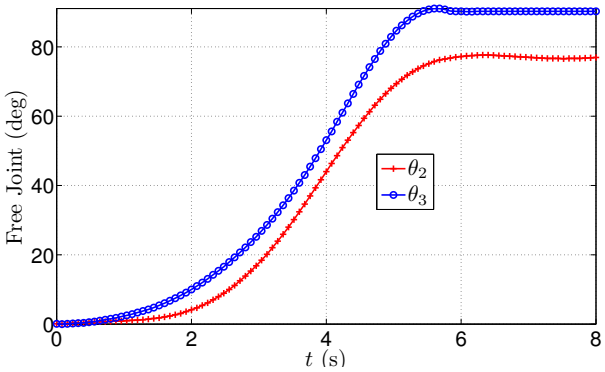

(b)

Fig. 11. Experimental results: (a) In-phase motion; (b) Out-of-phase motion

is to study the mechanism in a hybrid control framework, where the brakes serve as discrete inputs and the biaxial tilt trajectories serve as continuous inputs.

ACKNOWLEDGMENTS

The authors gratefully acknowledge The Boeing Company for supporting this work. The first author would like to thank Dr. Jun Ueda for many helpful discussions and comments.

REFERENCES

[1] B. Roy and H. Asada, "Dynamics and control of a gravity-assisted underactuated robot arm for assembly operations inside an aircraft wing-box," in *Robotics and Automation. Proceedings 2006 IEEE International Conference on*, June 2006, pp. 701–706.

[2] ——, "Closed loop control of a gravity-assisted underactuated robot arm with application to aircraft wing-box assembly," in *Proceedings of Robotics: Science and Systems*, Atlanta, GA, USA, June 2007.

[3] H. Arai, K. Tanie, and N. Shiroma, "Nonholonomic control of a three-dof planar underactuated manipulator," *Robotics and Automation, IEEE Transactions on*, vol. 14, no. 5, pp. 681–695, Oct 1998.

[4] J. Hauser and R. M. Murray, "Nonlinear controller for nonintegrable systems: the acrobot example," in *Proc. American Contr. Conf.*, 3-5 Nov 1990, pp. 669–671.

[5] M. W. Spong, "Swing up control of the acrobot," *Control Systems Magazine, IEEE*, vol. 15, no. 5, pp. 49–55, Feb 1995.

[6] K. M. Lynch, N. Shiroma, H. Arai, and K. Tanie, "Collision-free trajectory planning for a 3-dof robot with a passive joint," *International Journal of Robotics Research*, vol. 19, no. 12, pp. 1171–1184, 2000.

[7] M. Bergerman and Y. Xu, "Planning collision-free motions for under-actuated manipulators in constrained configuration space," in *Robotics and Automation. Proceedings 1997 IEEE International Conference on*, April 1997, pp. 549–555.

[8] T. Yoshikawa, K. Kobayashi, and T. Watanabe, "Design of a desirable trajectory and convergent control for 3-dof manipulator with a non-holonomic constraint," in *Robotics and Automation. Proceedings 2000 IEEE International Conference on*, 2000, pp. 1805–1810.

[9] G. Oriolo and Y. Nakamura, "Free-joint manipulators: motion control under second-order nonholonomic constraints," in *Intelligent Robots and Systems '91. Intelligence for Mechanical Systems, Proceedings IROS '91. IEEE/RSJ International Workshop on*, 3-5 Nov 1991, pp. 1248–1253.

[10] H. J. Sussmann, "A general theorem on local controllability," *SIAM Journal on Control and Optimization*, vol. 25, no. 1, pp. 158–194, 1987.